GENETICS, 2022, 221(1), iyac047
https://doi.org/10.1093/genetics/iyac047
Advance Access Publication Date: 28 March 2022
Neurogenetics

The PH/MyTH4/FERM molecule MAX-1 inhibits UNC-5 activity in the regulation of VD growth cone protrusion in *Caenorhabditis elegans*

Snehal S. Mahadik , Erik A. Lundquist *

Department of Molecular Biosciences, The University of Kansas, Lawrence, KS 66045, USA

*Corresponding author: Department of Molecular Biosciences, The University of Kansas, 1200 Sunnyside Avenue, Lawrence, KS 66045, USA. Email: erikl@ku.edu

Abstract

UNC-6/Netrin is a secreted conserved guidance cue that regulates dorsal-ventral axon guidance of *Caenorhabditis elegans* and in the vertebral spinal cord. In the polarity/protrusion model of VD growth cone guidance away from ventrally expressed UNC-6 (repulsion), UNC-6 first polarizes the growth cone via the UNC-5 receptor such that filopodial protrusions are biased dorsally. UNC-6 then regulates a balance of protrusion in the growth cone based upon this polarity. UNC-5 inhibits protrusion ventrally, and the UNC-6 receptor UNC-40/DCC stimulates protrusion dorsally, resulting in net dorsal growth cone outgrowth. UNC-5 inhibits protrusion through the flavin monooxygenases FMO-1, 4, and 5 and possible actin destabilization, and inhibits pro-protrusive microtubule entry into the growth cone utilizing UNC-33/CRMP. The PH/MyTH4/FERM myosin-like protein was previously shown to act with UNC-5 in VD axon guidance utilizing axon guidance endpoint analysis. Here, we analyzed the effects of MAX-1 on VD growth cone morphology during outgrowth. We found that *max-1* mutant growth cones were smaller and less protrusive than wild type, the opposite of the *unc-5* mutant phenotype. Furthermore, genetic interactions suggest that MAX-1 might normally inhibit UNC-5 activity, such that in a *max-1* mutant growth cone, UNC-5 is overactive. Our results, combined with previous studies suggesting that MAX-1 might regulate UNC-5 levels in the cell or plasma membrane localization, suggest that MAX-1 attenuates UNC-5 signaling by regulating UNC-5 stability or trafficking. Alternately, MAX-1 might inhibit UNC-5 independent of this known mechanism. We also show that the effects of MAX-1 in growth cone protrusion are independent of UNC-40/DCC, UNC-33/CRMP, and UNC-34/Enabled. In summary, in the context of growth cone protrusion, MAX-1 inhibits UNC-5, demonstrating the mechanistic insight that can be gained by analyzing growth cones during outgrowth in addition to axon guidance endpoint analysis.

Keywords: UNC-5; MAX-1; growth cone; *C. elegans*; UNC-6/Netrin

Introduction

In developing nervous system, axons must reach their target to form the functional neuronal connections. Growth cones are the dynamic structures present at the distal tip of a growing axons which respond to extracellular guidance cues, driving the forward or backward motion of axons (Tessier-Lavigne and Goodman 1996). Growth cones are actin-rich structures that consists of bundled actin filaments in filopodial protrusions and branched actin meshwork in lamellopodial protrusions (Zhou and Cohan 2004; Pak et al. 2008; Lowery and Van Vactor 2009). Various receptors present on the growth cone receive the guidance information, triggering a series of intracellular events that move the axon in correct direction (Tessier-Lavigne and Goodman 1996; Lowery and Van Vactor 2009).

In *Caenorhabditis elegans*, the extracellular guidance cue UNC-6 is secreted by ventral nerve cells and it mediates the dorsal ventral circumferential migration of growth cones and its axons with the help of its receptors UNC-5 and UNC-40 (Hedgecock et al. 1990; Ishii et al. 1992; Norris and Lundquist 2011). Previously, we have shown that there is a link between axon guidance and growth cone protrusion by UNC-6, UNC-40, and UNC-5 (Norris and Lundquist 2011). UNC-6 receptors UNC-40 and UNC-5 regulate growth cone protrusion. UNC-40 stimulates protrusion whereas UNC-5 inhibits protrusion, and asymmetric distribution of protrusive activity across the growth cone results in directed growth cone migration away from UNC-6/Netrin (the Polarity/Protrusion model) (Gujar et al. 2018).

max-1 (motor axon guidance-1) was previously isolated from a forward genetic screen for abnormal synapse formation and axon guidance defects in the GABAergic VD/DD motor neurons (Huang et al. 2002). In this study, MAX-1 was shown to act in the UNC-5 pathway to regulate repulsion of motor axons in *C. elegans*. A genetic study in zebrafish also suggested that *max-1* plays a role in regulating membrane localization of Ephrin3b protein, which provides guidance cue for the migration of endothelial cells during embryogenesis (Zhong et al. 2006). Another study showed that MAX-1 SUMOylation play an important role in regulating the trafficking and degradation of UNC-5 receptors during axon guidance which is required for UNC-5- mediated axon

repulsion (Chen et al. 2018). However, how MAX-1 functions in the growth cone during UNC-5-mediated repulsion is not clear. To address this issue, we used the genetic approach to analyze the double mutants and their growth cone phenotypes in VD neurons of *C. elegans*.

We found that *max-1* VD growth cones have reduced growth cone area and filopodial protrusion relative with wild type, and disrupted growth cone polarity such that dorsal polarity of filopodial protrusion is lost. We also found that *max-1* suppressed the excessively protrusive growth cones of *unc-5* hypomorphic mutations, consistent with the idea that MAX-1 might normally inhibit UNC-5 signaling in inhibition of growth cone protrusion. In the absence of MAX-1, elevated hypomorphic residual UNC-5 activity might inhibit growth cone protrusion resulting in small growth cones. We also found that *max-1* acted independently of other pathways that regulate growth cone protrusion, including *unc-40/DCC*, *unc-6/Netrin*, *unc-33/CRMP*, and *unc-34/Enabled*.

In contrast to our findings in the growth cone, endpoint axon guidance analysis showed that there is a synergistic interaction between *max-1*, *unc-5*, *unc-6*, and *unc-40*. Together, these results suggest that the linkage from growth cone structure to axon guidance has not been fully revealed by our growth cone analyses and likely involves additional factors in the growth cone that we have not assayed, such as dynamic aspects of filopodia formation and rate of growth cone outgrowth influenced by these molecules. However, analysis of growth cones during outgrowth in mutants can reveal new insights into the roles of these molecules not evident in postdevelopment axon guidance analyses.

Materials and methods

Genetic methods

Experiments were performed at 20°C using standard *C. elegans* techniques (Brenner 1974). Mutations were used LGI: *unc-40(n324)*; LGII: *juIs76* [*Punc-25::gfp*]; LGIV: *unc-5(e791, ev480,* and *e152)*, *unc-33(e204)*; LGV: *max-1(ju39, ju142,* and *lq148)*, *unc-34(gm104)*; LGX: *unc-6(ev400 and e78)*. The presence of mutations was confirmed by phenotype and sequencing. Chromosomal locations not determined. *myr::unc-5* [*Punc-25::myr::unc-5::gfp*].

max-1(lq148) was identified by whole-genome sequencing after EMS mutagenesis. *lq148* is a C to T transition that creates a glutamine to stop codon at codon 857 (position 13,099,591 on LGV). *lq148* failed to complement *max-1(ju39)* for the Unc phenotype and VD/DD axon guidance defects (data not shown), indicating that *lq148* is an allele of *max-1*.

Imaging of axon guidance defects

VD/DD neuron were visualized with *Punc-25::gfp* transgene, *juIs76* (Jin et al. 1999), which is expressed in GABAergic motor neurons including 13VDs and 6DDs. The commissure on the left side (VD1) was not scored. Remaining 18 commissures extend processes on the right side of the animal. Due to the fasciculation of some commissural processes, on an average only 16 VD/DD neurons were scored in a wild type. In case of mutants, only neurons emanating from the ventral nerve cord were scored for axon guidance defects (Gujar et al. 2017). Total axon guidance defects were calculated by counting all the axons which fails to reach the dorsal nerve cord, wandering at an angle of 45°, crossover between 2 neurons and, ectopic branching. Significance difference between 2 genotypes was determined by using Fisher's exact test with Bonferroni correction for multiple testing ($Padj < 0.05$).

Growth cone imaging and quantification

VD growth cones were imaged as described previously (Norris and Lundquist 2011). Wild-type animals are harvested 16 h posthatching at 20°C were placed on a 2% agarose pad and paralyzed with 5 mM sodium azide in M9 buffer. For mutant animals, due to the slower development the time point ranges between 17 and 21 h posthatching. Growth cones were imaged with Qimagine Rolera mGi camera on a Leica DM5500 microscope. Projections less than 0.5 μm in width were scored as filopodia. Growth cone area and filopodial length were quantified using ImageJ software. Quantification was done as described previously (Gujar et al. 2017). Significance of difference between 2 genotypes was determined by ANOVA with correction for multiple testing ($Padj < 0.05$).

To quantify polarity of filopodial protrusions, we divided the growth cone into 2 quadrants, dorsal and ventral with dorsal facing the dorsal nerve cord and ventral facing the ventral nerve cord. Then, we counted the number of filopodia in each quadrant and took the proportion of filopodia in dorsal and ventral quadrant. Significance difference between 2 genotypes was determined by using Fisher's exact test with Bonferroni correction for multiple testing ($Padj < 0.05$).

Results

MAX-1 is required for robust VD growth cone protrusion and polarity

MAX-1 is a member of the PH/MyTH4/FERM myosin-like family and contains an N-terminal coiled-coil region, followed by 2 pleckstrin homology domains (PH), a myosin tail homology region, and a FERM domain (Fig. 1a). *max-1* alleles were first identified in a screen for abnormal synapse formation and axon guidance defects in the GABAergic VD/DD motor neurons (Huang et al. 2002). *max-1(ju39)* is a 28-nucleotide deletion within the second exon which cause a frameshift after amino acid 58, *max-1(ju142)* is an 81-nucleotide deletion at the exon/intron boundary of the fourth exon (Huang et al. 2002), and *max-1(lq148)* is a C to T transition in the penultimate *max-1* exon resulting in a premature stop codon at glutamine 857 (Fig. 1, a and b). Growth cone analysis indicated that *lq148* is likely a *max-1* hypomorphic allele, whereas *ju142* is a likely null (see below).

MAX-1 was previously shown to act with the UNC-6/Netrin receptor UNC-5 in dorsal VD/DD motor neuron axon guidance, and in parallel to the UNC-40/DCC Unc-6/Netrin receptor (Huang et al. 2002). These studies involved endpoint axon guidance analysis, but did not assay the growth cone during outgrowth. At the growth cone level, UNC-5 controls polarity of GABAergic growth cone protrusion as well as extent of protrusion (the polarity/protrusion model) (Norris and Lundquist 2011; Norris et al. 2014; Gujar et al. 2018). Given the genetic interaction of *max-1* with *unc-5*, we endeavored to understand the role of MAX-1 in GABAergic growth cone polarity and protrusion.

We first confirmed the GABAergic dorsal axon guidance defects in *max-1* mutants. The 19 VD/DD motor neurons cell bodies resides in the ventral nerve cord (Fig. 1c). Axons of the VD and DD neurons first extend anteriorly in the ventral nerve cord, and then turn dorsally to extend commissural to the dorsal nerve cord (Figs. 1c and 2a). In wild-type animals, on average 16 commissures were observed, due to the fasciculation of some processes as single commissures (Fig. 1d). As previously reported (Huang et al. 2002), *max-1* mutants display VD/DD axon guidance

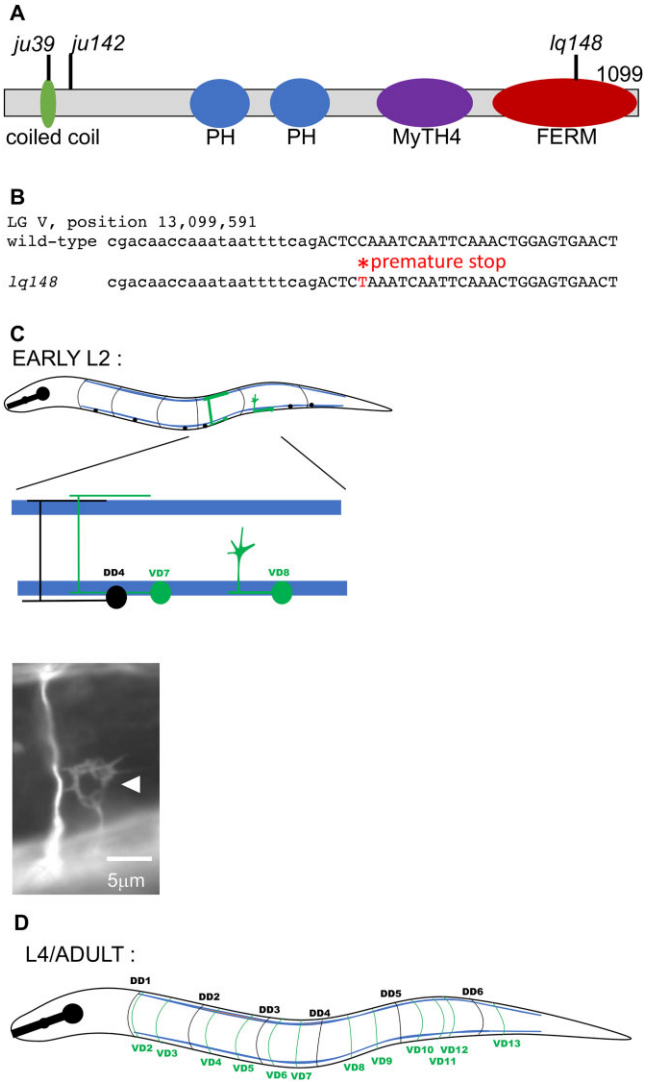

Fig. 1. MAX-1 and VD neurons. a) *max-1* alleles and location of their molecular lesions. b) Sequence comparison of *lq148* allele to the wild type. *lq148* shows change from C to T shown in red. c) Modified from Gujar et al. 2017. Diagram of early L2 larva of *C. elegans* hermaphrodite highlighting the structure and position of DD (black) and VD (green) motor neuron and axons. Dorsal is up, and anterior is left. Blue line represents the dorsal and ventral muscle quadrant. While migrating toward dorsal nerve cord VD neuron extends a growth cone with protrusive morphology and dynamic filopodial protrusions (VD8). VD7 shows the final structure of VD neurons in wild type. Fluorescent micrograph shows a wild-type VD growth cone marked by an arrowhead. Scale bar represents 5 µm. d) Modified from Gujar et al. 2017. Diagram of L4 hermaphrodite after VD axon outgrowth is complete. VD1 is not shown. 18 commissures shown as black lines and axon guidance of these 18 commissures were scored. Of these 18 commissures on the right side, 2 (DD1 and VD2) extend as single fascicle. Other fascicles occasionally extend as single fascicles as well, resulting in an average of 16 commissures per wild-type animal.

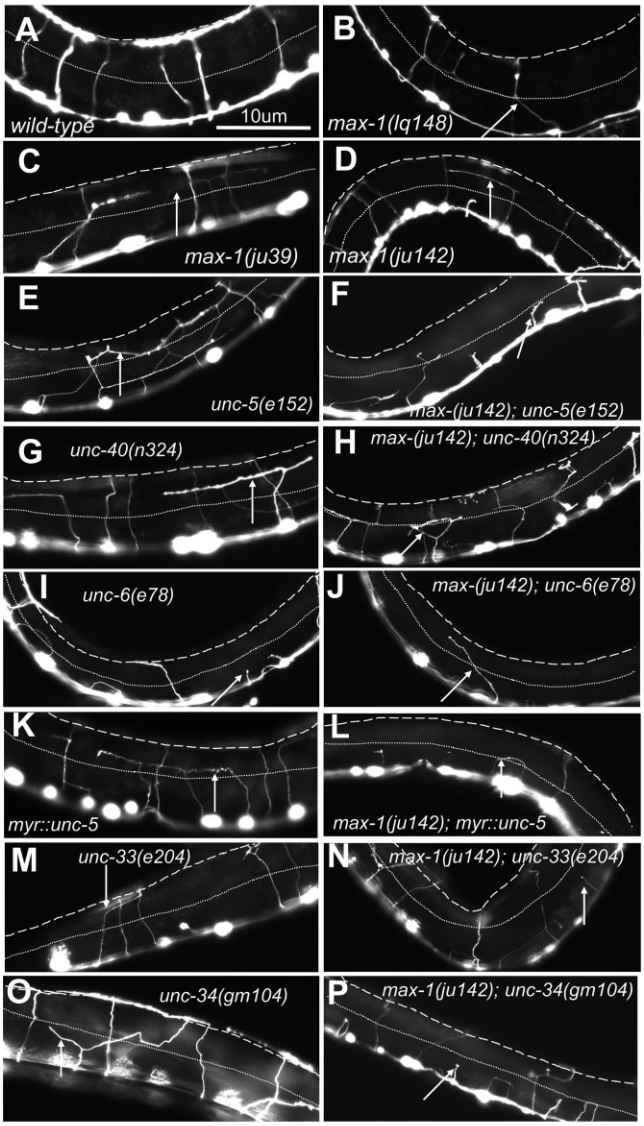

Fig. 2. VD/DD axon guidance defects. Shown are fluorescent micrographs of the *Punc-25::gfp* transgene *juIs76* expressed in the VD/DD neurons of L4 animals a) wild type, b–d) *max-1(lq48)*, *max-1(ju39)*, *max-1(ju42)*, e and f) *unc-5(e152)*, *max-1(ju142)*; *unc-5(e152)*, g and h) *unc-40(n324)*, *max-1(ju142)*; *unc-40(n324)*, i and j) *unc-6(e78)*, *max-1(ju142)*; *unc-6(e78)*, k and l) *myr::unc-5*, *max-1(ju142)*; *myr::unc-5*, m and n) *unc-33(e204)*, *max-1(ju142)*; *unc-33(e204)*, and o and p) *unc-34(gm104)*, *max-1(ju142)*; *unc-34(gm104)*. The lateral midline is indicated by dashed white dots. Dorsal nerve cord is marked by dashed white line. Dorsal is up. White arrows are indicating axon guidance defects in each genotype. Scale bar 10 µm.

defects (21–25%), including axon wandering, failure to reach the dorsal nerve cord, and ectopic axon branching (Figs. 2, b–d and 3).

We next analyzed VD growth cone morphology in *max-1* mutants. In the early L2 larval stage, VD axons extend anteriorly in the ventral nerve cord, and then turn dorsally to extend a commissure to the dorsal nerve cord (Fig. 1c). During this commissural extension, between the lateral midline and the ventral and dorsal nerve cords, wild-type VD growth cones display a robust growth cone body and filopodial protrusions (Figs. 1c and 4, a, b, andd), with an average growth cone area of 4.6 μm^2, and an average filopodial length of 0.95 µm (Fig. 4, a and b). Furthermore, filopodial protrusions were biased to the dorsal half of the growth cone (Fig. 4, c and d). In *max-1* mutants, VD growth cones were significantly smaller than wild type (Fig. 4, aand d–f). Filopodial protrusions were significantly shorter in *max-1(ju142)* (Fig. 4, b and f). *max-1(lq148)* and *max-1(ju39)* also displayed shorter filopodia, but not significantly so when corrected for multiple testing (*Padj* = 0.07, Fig. 4b).

Filopodial protrusions were still biased to the dorsal, but less so than wild type in all 3 alleles, and significantly less so in *ju142* (Fig. 4, c and f). A *max-1(lq148/ju142) trans*-heterozygote displayed

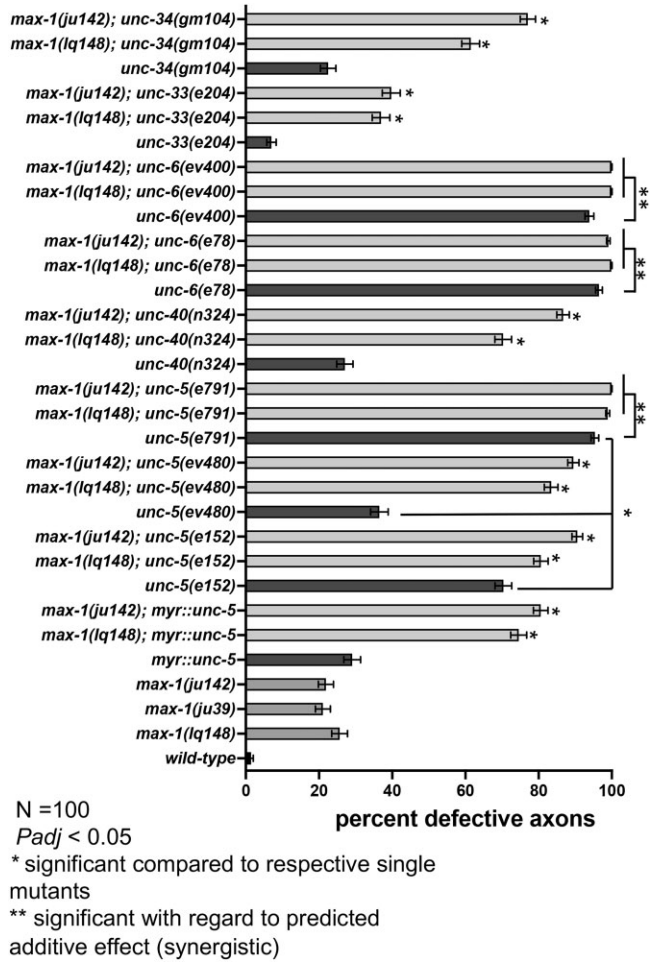

Fig 3. Quantification of VD/DD axon guidance defects. Quantification of total axons that failed to reach the dorsal nerve cord of L4 hermaphrodite in wild type and mutants indicated along the Y axis. Error bars represents 2× standard error of proportion. Asterisks indicate significance as determined by Fisher's exact test with Bonferroni correction (*Padj*) compared to single mutants alone of the predicted additive effect of double mutants.

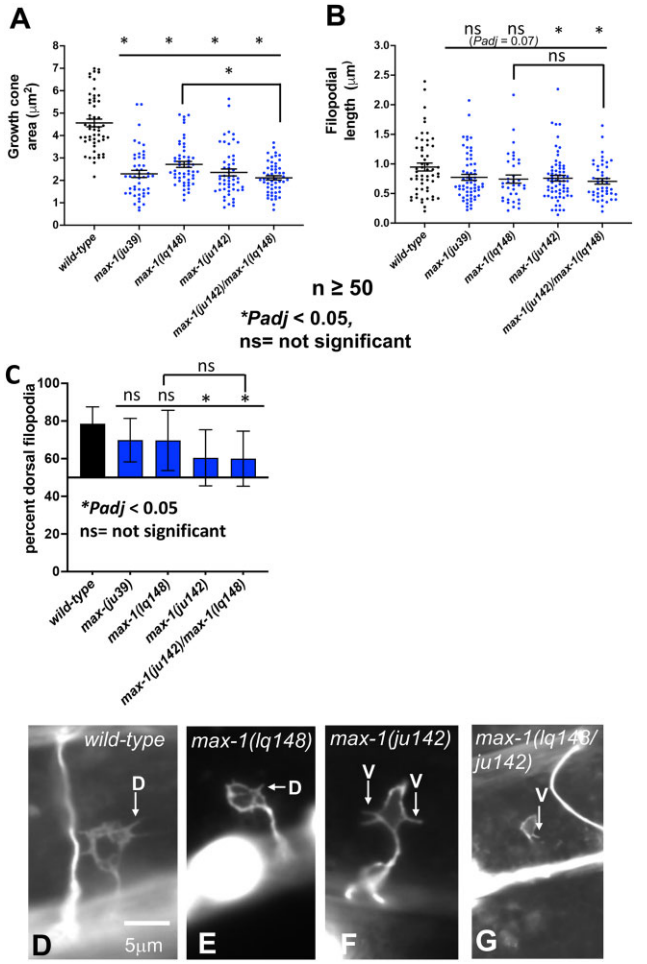

Fig. 4. Growth cone analysis in *max-1* mutants. At least 50 growth cones were scored in each genotype. a and b) Quantification of VD growth cone area and filopodial length (see *Materials and Methods*). Each point represents an individual growth cone of filopodium. a) Area of growth cone, in μm^2. b) Filopodial length, in μm. Error bars indicate standard error of mean. Single asterisks (*) indicates *Padj* < 0.05; Significance is determined by using one-way ANOVA with multiple comparison. A black line indicates comparison to wild type, whereas brackets denote comparisons between indicated genotypes. c) A graph showing the % of dorsally directed filopodial protrusions in VD growth cones of different genotypes (see *Materials and Methods*). The X-axis is set at 50%, such that bars extending above the X-axis represents above 50%, and bars that extends below represents below 50%. In wild type, a majority of filopodia (78%) extended from the dorsal half of the growth cone. Single asterisks (*) indicate the significant *Padj* < 0.05 compared to wild type. A black line indicates comparison to wild type, whereas brackets denote comparisons between indicated genotypes. Error bar represents 2× standard error of proportion. Significance is determined by Fisher's exact test and multiple comparison was done by performing Bonferroni correction (*Padj*). d–g) Fluorescence micrographs of wild-type and mutant VD growth cones expressing *Punc-25::gfp*. d–g) Image of wild-type, *max-1(lq148)*, *max-1(ju142)*, and *max-1(lq148/ju142)* VD growth cones, respectively. The arrows point to filopodial protrusions (D = dorsal protrusion; V = ventral protrusion). Scale bar: 5 μm.

significantly reduced growth cone area compared to *max-1(lq148)* alone (Fig. 4, a and g), suggesting that *max-1(lq148)* is a hypomorphic allele and retains some *max-1* activity. In sum, *max-1* was required for robust growth cone protrusion, and for growth cone polarity.

max-1 suppresses excessive growth cone protrusion in hypomorphic *unc*-5 mutants

Our results suggest that the effect of loss of MAX-1 on VD growth cones resembles constitutive UNC-5 activity (small growth cones with reduced protrusion) (Norris et al. 2014). *unc-5(e152)* and *unc-5(ev480)* are hypomorphic alleles, incomplete loss-of-function mutations with weaker Unc phenotypes than null alleles (Merz et al. 2001; Killeen et al. 2002). VD/DD axon guidance defects in *unc-5(e152)* and *unc-5(ev480)* were significantly weaker than those in the null allele *unc-5(e791)* (Fig. 3). The hypomorphic nature of *unc-5(e152)* and *unc-5(ev480)* suggests that some UNC-5 function is retained in these mutants.

VD growth cones in *unc-5(e152)* and *unc-5(ev480)* displayed increased growth cone area and filopodia length similar to the *unc-5(e791)* null mutant (Fig. 5, a, b, d, and g), consistent with the previously described role of UNC-5 in inhibiting VD growth cone protrusion (Norris and Lundquist 2011; Norris et al. 2014; Gujar et al. 2018). *unc-5* hypomorph growth cones were also unpolarized (Fig. 5c), with loss of dorsal bias of growth cone protrusion as previously reported for *unc-5* mutants.

VD growth cones of double mutants of *max-1(lq148 and ju142)* with hypomorphic *unc-5(e152 and ev480)* displayed reduced growth cone area and filopodial length relative to *unc-5* alone and in fact resembled the small growth cones of *max-1* alone

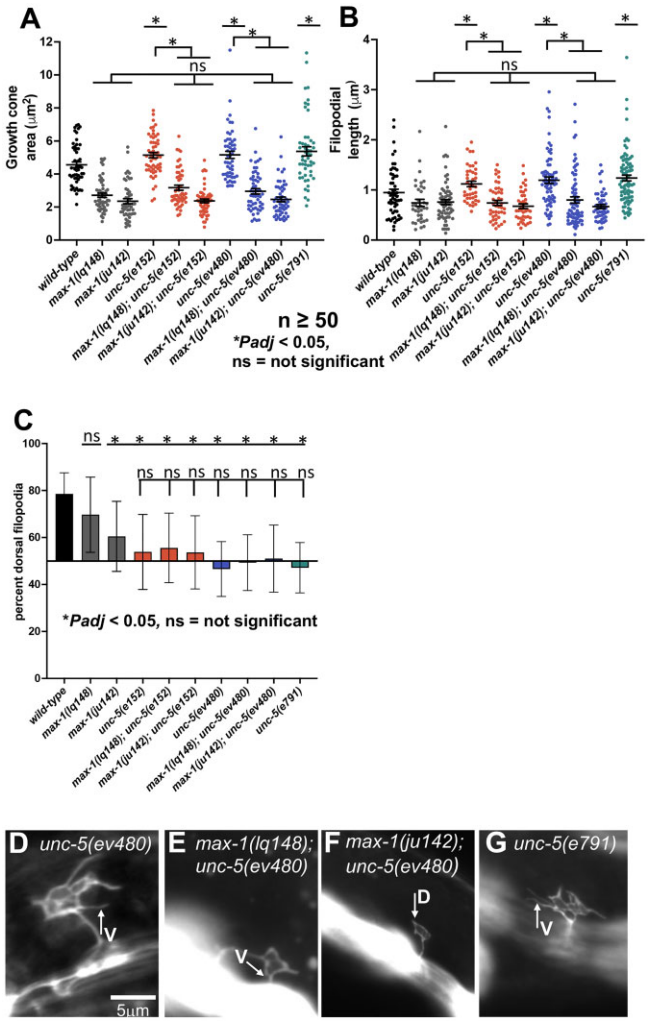

Fig. 5. Growth cone analysis in *unc*-5 and *max*-1 mutants. a and b) Quantification of VD growth cone area and filopodial length as described in Fig. 4. c) A graph showing the % of dorsally-directed filopodial protrusions in VD growth cones of different genotypes as described in Fig. 4. d–g) Fluorescence micrographs of mutant VD growth cones expressing *Punc-25::gfp*. d–g) Image of *unc-5(ev480)*, *max-1(lq148)*; *unc-5(ev480)*, *max-1(ju142)*; *unc-5(ev480)*, *unc-5(e791)* VD growth cones respectively. The arrows point to filopodial protrusions (D = dorsal protrusion; V = ventral protrusion). Scale bar: 5 μm.

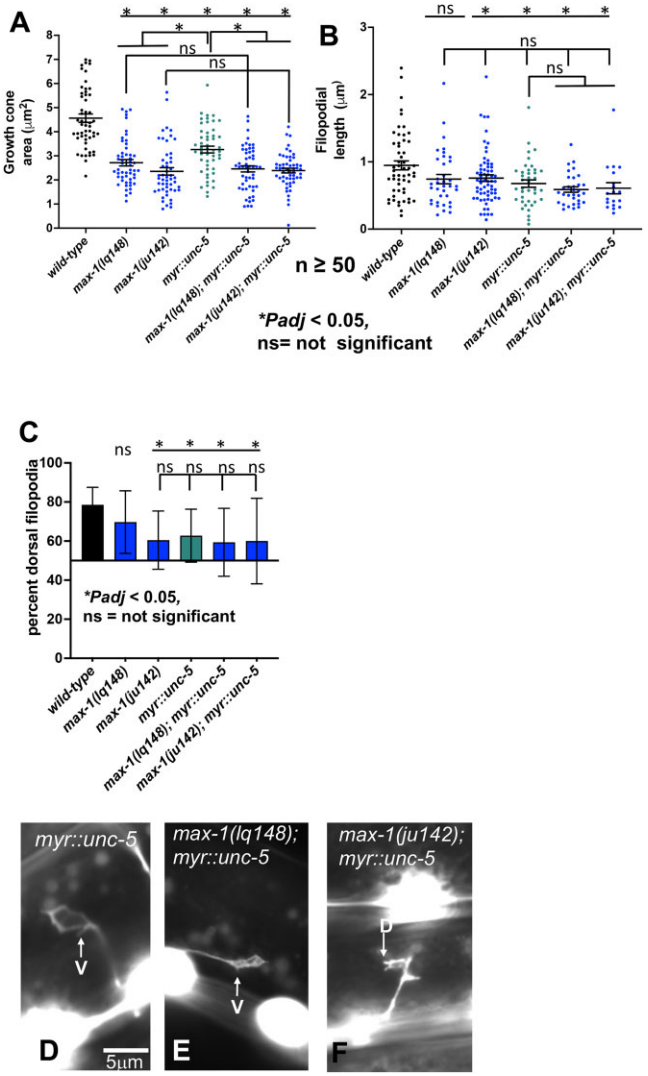

Fig. 6. Growth cone analysis in *myr::unc*-5 and *max*-1 double mutants. a and b) Quantification of VD growth cone area and filopodial length as described in Fig. 4. c) A graph showing the % of dorsally directed filopodial protrusions in VD growth cones of different genotypes as described in Fig. 4. d–f) Fluorescence micrographs of wild-type and mutant VD growth cones expressing *Punc-25::gfp*. d–f) Image of *myr::unc*-5, *max-1(lq148)*; *myr::unc*-5, and *max-1(ju142)*; *myr::unc*-5 VD growth cones, respectively. The arrows point to filopodial protrusions (D = dorsal protrusion; V = ventral protrusion). Scale bar: 5 μm.

(Fig. 5, a, b, e, and f). The *unc*-5*(e791)* null mutant displayed large and protrusive growth cones (Fig. 5, a, b, and g), but growth cones of *max*-1; *unc*-5*(e791)* double mutants could not be scored because no VD growth cones emerged from the ventral nerve cord in these animals (data not shown). These results indicate that loss of *max*-1 suppressed the excessive VD growth cone area and filopodial length observed in hypomorphic *unc*-5 mutants. Growth cone polarity defects in *max*-1; *unc*-5 double mutants resembled the *unc*-5 mutants alone (Fig. 5c). These results suggest that MAX-1 might normally inhibit UNC-5, and that residual *unc*-5 activity in the *unc*-5 hypomorphic alleles might be increased in *max*-1 mutants.

Expression of constitutively active, ligand independent *myr::unc*-5 in the VD neurons resulted in reduced growth cone area and filopodial length (Norris et al. 2014) (Fig. 6, a, b, and d). *max*-1 mutants showed significantly more severe effects on area (Fig. 6, a and b). *max*-1; *myr::unc*-5 double mutants resembled *max*-1 alone, with reduced growth cone area compared to *myr::unc*-5 alone (Fig. 6, a, b, e, and f). VD growth cone polarization of *max*-1; *myr::unc*-5 resembled single mutants alone (Fig. 6c). *max*-1; *myr::unc*-5 resembling *max*-1 alone is consistent with increased activity of wild-type UNC-5 in *max*-1 mutants independent of *myr::unc*-5.

max-1; *unc*-40 and *max*-1; *unc*-6 double VD growth cones display reduced protrusion similar to *max*-1 alone

The UNC-6/Netrin receptor UNC-40/DCC has a dual role in controlling growth cone protrusion. It acts as a heterodimer with UNC-5 to inhibit protrusion, and as a homodimer to stimulate protrusion (Norris and Lundquist 2011; Norris et al. 2014; Gujar et al. 2018). *unc*-40*(n324)* null mutant displayed similar growth cone area compared to wild-type, but shortened growth cone filopodial protrusions (Fig. 7, a, b, and d). This moderate phenotype likely reflects the dual role of UNC-40 in protrusion. *max*-1; *unc*-40 double mutants growth cones displayed reduced growth cone

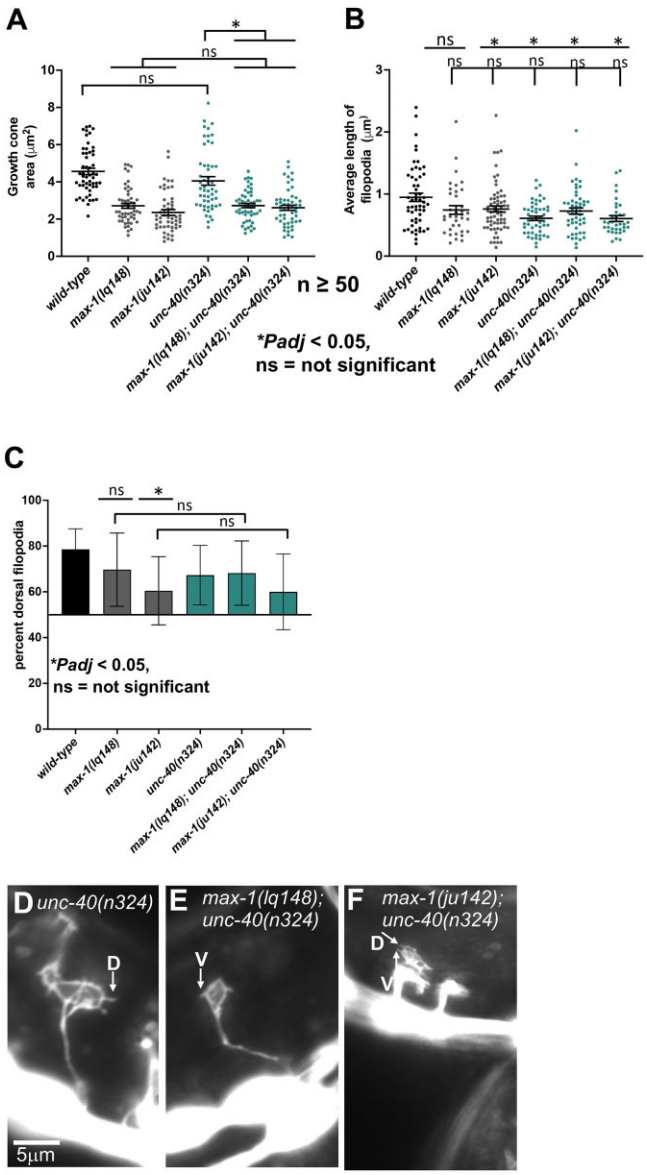

Fig. 7. Growth cone analysis in *unc-40* and *max-1* mutants. a and b) Quantification of VD growth cone area and filopodial length as described in Fig. 4. c) A graph showing the % of dorsally directed filopodial protrusions in VD growth cones of different genotypes as described in Fig. 4. d–f) Fluorescence micrographs of mutant VD growth cones expressing *Punc-25::gfp*. d–f) Image of *unc-40(n324)*, *max-1(lq148)*; *unc-40(n324)*, *max-1(ju142)*; *unc-40(n324)* VD growth cones, respectively. The arrows point to filopodial protrusions (D = dorsal protrusion; V = ventral protrusion). Scale bar: 5 μm.

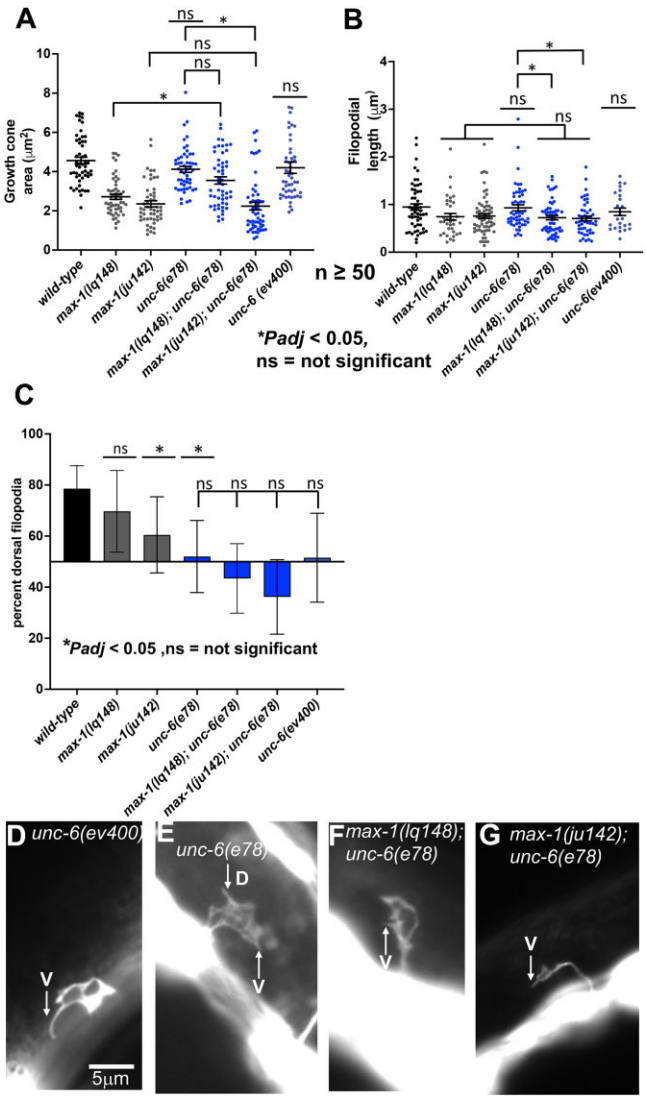

Fig. 8. Growth cone analysis in *unc-6* and *max-1* mutants. a and b) Quantification of VD growth cone area and filopodial length as described in Fig. 4. c) A graph showing the % of dorsally directed filopodial protrusions in VD growth cones of different genotypes as described in Fig. 4. d–g) Fluorescence micrographs of mutant VD growth cones expressing *Punc-25::gfp*. d–g) Image of *unc-6(ev400)*, *unc-6(e78)*, *max-1(lq148)*; *unc-6(e78)*, *max-1(ju142)*; *unc-6(e78)* VD growth cones, respectively. The arrows point to filopodial protrusions (D = dorsal protrusion; V = ventral protrusion). Scale bar: 5 μm.

area similar to *max-1* and reduced filopodial length similar to *unc-40* and *max-1* (Fig. 7, a, b, e, and f). Growth cone polarity in *max-1*; *unc-40* double mutants resembled *max-1* alone (Fig. 7c). This additive phenotype suggests that MAX-1 acts independently of UNC-40 in growth cone protrusion. In other words, the small growth cone phenotype of *max-1* does not require functional UNC-40.

As reported previously, *unc-6(ev400)* null mutation had no significant effect on VD growth cone area and filopodial length, but caused strong growth cone polarity defects (Fig. 8, a–d). Growth cones of *max-1*; *unc-6(ev400)* double mutants could not be scored because none emerged from the ventral nerve cord (data not shown). The hypomorphic allele *unc-6(e78)* is a substitution of cysteine to tyrosine in V-3 domain, which disrupts the interaction between UNC-6 and UNC-5 (Lim and Wadsworth 2002; Norris and Lundquist 2011). Dorsal growth is more strongly affected than ventral growth in *unc-6(e78)*. Previous results showed that *unc-6(e78)* mutants displayed unpolarized VD growth cones with excessive protrusion (Norris and Lundquist 2011). When *unc-6(e78)* was scored again for these studies, growth cones did not show excessive protrusion (Fig. 8, a and b) but were still unpolarized as found previously (Fig. 8c).

max-1(ju142); *unc-6(e78)* VD growth cone area and filopodia length was reduced compared to *unc-6(e78)* and resembled *max-1(ju142)* alone (Fig. 8, a, b, and g). Growth cone area of *max-1(lq148)*; *unc-6(e78)* was not significantly reduced compared to *unc-6(e78)* alone, possibly due to the hypomorphic nature of *max-1(lq148)*. Surprisingly, *max-1(lq148)*; *unc-6(e78)* area was significantly larger than *max-1(lq148)* alone. We do not understand the nature of this interaction, but it might have to do with the

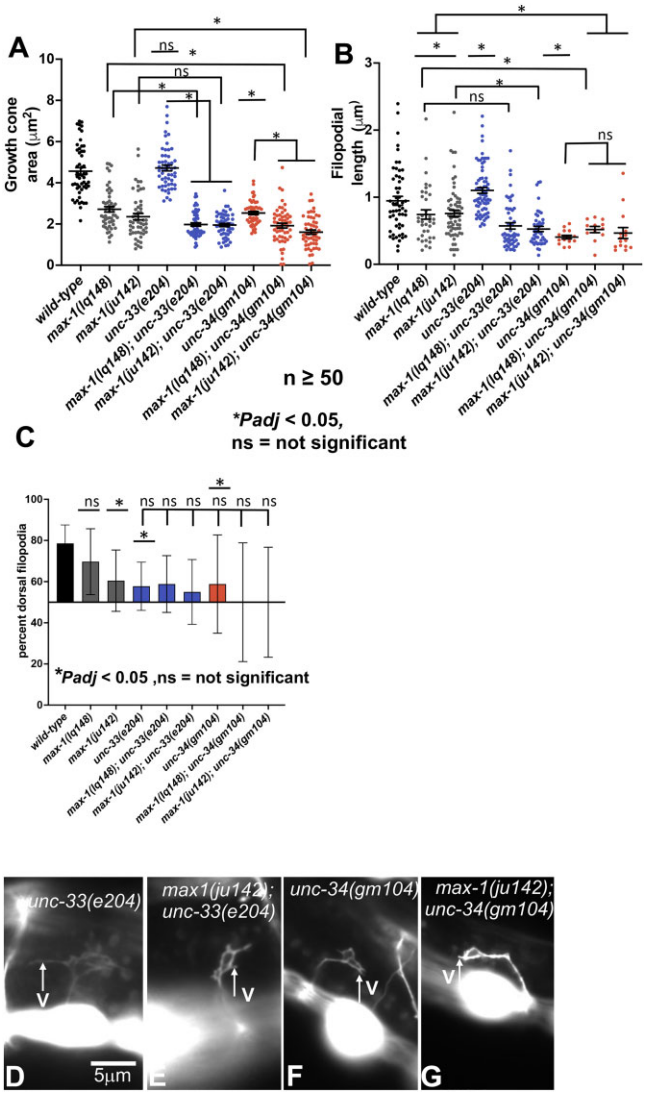

Fig. 9. Growth cone analysis in *unc-33*, *unc-34*, and *max-1* mutants. a and b) Quantification of VD growth cone area and filopodial length as described in Fig. 4. c) A graph showing the % of dorsally directed filopodial protrusions in VD growth cones of different genotypes as described in Fig. 4. d–g) Fluorescence micrographs of mutant VD growth cones expressing *Punc-25::gfp*. d–g) Image of *unc-33(e204)*, *max-1(ju142)*; *unc-33(e204)*, *unc-34(gm104)*, *max-1(ju142)*; *unc-34(gm104)* VD growth cones, respectively. The arrows point to filopodial protrusions (D = dorsal protrusion; V = ventral protrusion). Scale bar: 5 μm.

hypomorphic nature of both alleles. Growth cone polarity of *max-1*; *unc-6(e78)* resembled *unc-6(e78)* alone (Fig. 8c).

max-1; *unc-33* mutants display reduced growth cone protrusion similar to *max-1* alone

Previous studies showed that UNC-5 normally restricts microtubule + ends from growth cones via the microtubule interacting molecule UNC-33/CRMP, and that microtubules have a pro-protrusive role in the growth cone (Gujar et al. 2018, 2019). As reported previously, *unc-33(e204)* mutants displayed larger-than wild-type VD growth cones with significantly longer filopodia (Gujar et al. 2018) (Fig. 9, a, b, and d) and a loss of growth cone polarity of filopodial protrusions (Fig. 9c). *unc-33* growth cone area was not significant when corrected for multiple testing (Fig. 9a). Loss of *max-1* significantly reduced growth cone area and filopodial length in *unc-33(e204)* (Fig. 9, a, b, d, and e). This suggests that functional UNC-33 is not required for inhibition of protrusion in *max-1* mutants.

unc-33; *max-1(lq148)* growth cones were significantly smaller than *max-1(lq148)* alone and resembled the null *max-1(ju142)* (Fig. 9a), and *unc-33*; *max-1(ju142)* filopodia were significantly shorter that *max-1(ju142)* alone (Fig. 9b). We do not understand this increase in severity, but multiple pathways operate downstream of UNC-5 to inhibit growth cone protrusion (Gujar et al. 2017, 2018, 2019). One of these parallel pathways might be more active in the absence of UNC-33. No significant difference in growth cone polarity in *unc-33*; *max-1* mutants compared to *unc-33* alone were observed (Fig. 9c). In any event, functional UNC-33 is not required for inhibited protrusion in *max-1* mutants.

unc-34 mutants have small growth cones with reduced filopodial protrusion

The actin-nucleating protein UNC-34/Enabled was required for robust growth cone protrusion of the PQR dendritic growth cone (Norris et al. 2009).

VD growth cones in *unc-34(gm104)* were significantly smaller than wild type with very few filopodial protrusions (Fig. 9, a, b, and f). Indeed, the 50 growth cones analyzed displayed a total of 15 filopodial protrusions (Fig. 9b). These results suggest that UNC-34/Enabled is required for robust VD growth cone and filopodial protrusion, consistent with a role as an actin nucleating factor.

Filopodial protrusions were also unpolarized in *unc-34* (Fig. 9c), suggesting that UNC-34/Enabled is required for growth cone polarity. However, the low number of filopodia present in *unc-34* decreases confidence in this result and led to a very large standard error of the proportion.

Growth cone area was significantly reduced in *max-1*; *unc-34* double mutants compared to single mutants alone (Fig. 9, a, f, and g). Filopodial length resembled *unc-34* alone. As both mutants displayed small growth cones, this could be an additive effect, or *unc-34* might act partially in parallel to *max-1*. No significant effect on polarity was observed in *unc-34*; *max-1* double mutants compared to single mutants alone (Fig. 9c).

max-1 enhances VD/DD axon guidance defects of *unc-5*, *unc-6*, and *unc-40*

Previous studies demonstrated strong genetic interactions between *max-1* and *unc-5*, *unc-6*, *and unc-40* in endpoint axon guidance analyses (Huang et al. 2002). *max-1* mutations enhanced hypomorphic *unc-5* alleles, and synergized with *unc-40(null)* for VD/DD axon guidance defects. *unc-5* and *unc-6*, but not *unc-40*, were dominant enhancers of *max-1*. Overexpression of *unc-5* and *unc-6* but not *unc-40* could suppress *max-1*. Finally, overexpression of *max-1* caused axon guidance defects that could be suppressed by overexpression of *unc-5* and *unc-6* but not *unc-40*. Together, these data suggest that MAX-1 acts in the UNC-6 and UNC-5 pathway, possibly in parallel to UNC-40.

We repeated VD/DD axon guidance endpoint analysis using the alleles in which VD growth cones were analyzed. *max-1* double mutants with *unc-5* and *unc-6* null alleles showed a complete failure of VD/DD axon guidance (Figs. 2 and 3), consistent with previous results (Huang et al. 2002) and with our observation of no VD growth cones exiting the ventral nerve cord in these double mutants. *max-1*; *unc-6(e78)* also showed almost complete axon guidance failure (Fig. 3). *max-1* enhanced VD/DD axon guidance defects of the *unc-5(e152)* and *unc-5(ev480)* hypomorphic alleles, with the *max-1*; *unc-5(ev480)* enhanced synergistically

(Figs. 2 and 3). This is also consistent with previous results (Huang et al. 2002). Axon guidance defects of *unc-40(n324)* were synergistically enhanced by *max-1* (Figs. 2 and 3), consistent with previous results (Huang et al. 2002).

We also performed VD/DD axon guidance analysis in the double mutant of *max-1*; *unc-33* and *max-1*; *unc-34*. *unc-33(e204)* displayed a strong Unc phenotype, yet caused only 7% of axon guidance defects. *unc-34(gm104)* also displayed a strong Unc phenotype and caused 23% guidance defects. Axon guidance defects of double mutant of *max-1*; *unc-33* and *max-1*; *unc-34* were significantly more severe than each single mutant (Figs. 2 and 3).

Discussion

MAX-1 regulates VD growth cone area, filopodial length, and dorsal polarization of filopodia

Previous results using VD/DD dorsal axon guidance endpoint analysis indicated that MAX-1 acts with UNC-5 and UNC-6, and in parallel to UNC-40. Our VD/DD axon guidance endpoint analysis presented here supports this conclusion. However, our analysis of VD growth cone morphology during dorsal outgrowth suggests that *max-1* and *unc-5* might have opposing roles. The VD growth cones of *unc-5* hypomorphic mutants displayed excessive protrusion. The growth cones were larger than wild type with longer filopodial protrusions. This is consistent with the known role of UNC-5 in inhibiting VD growth cone protrusion (Norris and Lundquist 2011; Norris et al. 2014; Gujar et al. 2018). *max-1* growth cones displayed an opposite phenotype. They were smaller than wild type with shorter filopodial protrusions, suggesting that MAX-1 was required for robust growth cone protrusion. Thus, in at least some aspects of growth cone outgrowth during axon guidance, UNC-5 and MAX-1 might have opposing roles. *max-1* alone mutants affected growth cone polarity, and did not suppress growth cone polarity defects of UNC-5 mutants. Growth cone polarity in *max-1* mutants might act independently of *unc-5*.

MAX-1 might attenuate UNC-5 signaling in growth cone protrusion

unc-5 hypomorphic VD growth cones displayed excessive protrusion, consistent with the role of UNC-5 normally inhibiting growth cone protrusion. However, these hypomorphic alleles retain some UNC-5 activity, as the VD/DD axon guidance defects are significantly less severe than *unc-5* null mutants. VD growth cones of *max-1*; *unc-5(hypomorphic)* resembled the small, less protrusive growth cones of *max-1* alone. This suggests that MAX-1 is required for the large, overly protrusive growth cones in *unc-5* mutants. It is possible that MAX-1 acts in a parallel pathway to drive protrusion, such as UNC-40, but genetic analyses suggest that MAX-1 acts in parallel to UNC-40 in the UNC-5 pathway. Rather, we speculate that MAX-1 normally attenuates UNC-5 signaling in growth cone protrusion (Fig. 10). In a *max-1* mutant, UNC-5 might be overly active, leading to reduced growth cone protrusion. In an *unc-5* hypomorph, MAX-1 might be attenuating what little UNC-5 function remains, resulting in large, protrusive growth cones. In a *max-1*; *unc-5(hypomorphic)* double mutant, *max-1* is no longer attenuating residual UNC-5 activity, which inhibits growth cone protrusion, resulting in suppression of excessive protrusion in *unc-5(hypomorphic)* mutations. If this was the case, we expect that *max-1* would not suppress *unc-5(null)*, because there would be no residual UNC-5 activity. However, we were unable to score VD growth cones in these double mutants, as none emerged from the ventral nerve cord. The phenotypic resemblance of *max-1*mutants and constitutively active *myr::unc-5* growth cones is consistent with an opposing role of MAX-1 and UNC-5. Furthermore, previous work showing that overexpression of UNC-5 can compensate for overexpression of MAX-1 in VD/DD axon guidance (Huang et al. 2002) is consistent with opposing roles, which we discovered in growth cone protrusion.

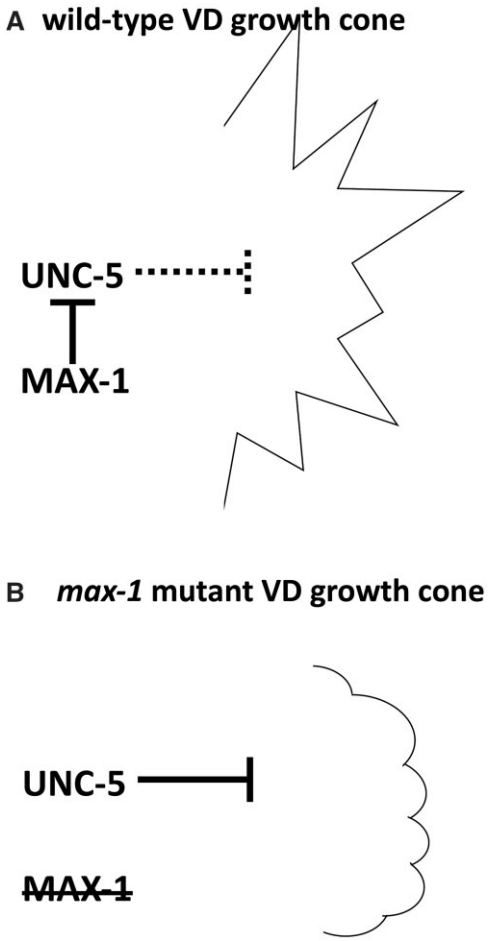

Fig 10. MAX-1 attenuates UNC-5 signaling in VD growth cones. a) In wild type, presence of MAX-1 regulates over activity of UNC-5 by attenuating UNC-5 signaling. This could be done by targeting UNC-5 for lysosomal degradation. Finally leads to the formation of dynamic growth cones required to reach to the dorsal nerve cord. b) In *max-1* mutants, due to the absence of MAX-1 activity now there is no regulation on UNC-5 activity. This over activity of UNC-5 leads to the formation of small, nonprotrusive . growth cones, which prevents VD neurons from reaching to the dorsal nerve cord and ultimately resulting in axon guidance defects.

Previous studies suggest that SUMOylated MAX-1 controls the interaction of the ABP-3/AP-3 complex β molecule with UNC-5, which targets UNC-5 to the lysosome for degradation (Chen et al. 2018). In this model, MAX-1 is constitutively bound to UNC-5 until it is SUMOylated, which allows ABP-3 to bind to UNC-5 and target it for lysosomal degradation. This model predicts that loss of MAX-1 would result in reduced UNC-5 activity, yet we show evidence here of increased UNC-5 activity in *max-1* mutants. Possibly, SUMOylated MAX-1 also participates in lysosomal trafficking such that in a *max-1* mutant, UNC-5 is not degraded, resulting in high levels of UNC-5 in the growth cone and inhibited growth cone protrusion. Alternatively, MAX-1 might inhibit UNC-5 through a mechanism independent of ABP-3 and lysosomal

targeting, such as directly binding to and inhibiting UNC-5 signaling directly.

MAX-1 acts independently of UNC-6/Netrin, UNC-40/DCC, and known cytoskeletal mechanisms

unc-6; *max-1* and *unc-40*; *max-1* growth cones resembled *max-1* mutants alone, suggesting that MAX-1 acts independently of UNC-6/Netrin and its receptor UNC-40/DCC. This is consistent with a specific effect of MAX-1 on inhibiting UNC-5 activity.

UNC-33/CRMP inhibits growth cone protrusion downstream of UNC-5 by restricting microtubule + end entry into the growth cone (Gujar et al. 2018), and as a result, *unc-33* mutants display large, overly protrusive growth cones. *max-1*; *unc-33* mutants resembled *max-1* alone, with smaller growth cones and shorter filopodial protrusions. Thus *unc-33* is not required for the small growth cone phenotype in *max-1* mutants. Possibly, in *unc-33*; *max-1* double mutants, overactive UNC-5 engages one of the pathways downstream that acts in parallel to UNC-33, such as the FMOs and actin (Gujar et al. 2017), resulting in small growth cones and short filopodia.

Here we show that actin-nucleating factor UNC-34/Enabled is required for robust VD growth cone protrusion and filopodia formation, similar to what we described previously for the PQR dendritic growth cone (Norris et al. 2009). UNC-34/Enabled might stimulate actin polymerization and thus growth cone protrusion, consistent with its role as an actin nucleation factor. Growth cone area was significantly reduced in *max-1*; *unc-34* double mutant VD growth cones compared to single mutants alone. As both mutants have reduced growth cone area, this could be an additive effect. Alternatively, *unc-34* and *max-1* might act partially in parallel to control growth cone area.

These results suggest that MAX-1 acts independently of UNC-40/DCC, UNC-33/CRMP, and UNC-34/Enabled and might act specifically with UNC-5 to regulate growth cone protrusion, consistent with biochemical studies (Chen et al. 2018).

The relationship of growth cone morphology to endpoint axon guidance phenotypes

Previous results (Huang et al. 2002) and results presented here using endpoint axon guidance analysis indicate that MAX-1 and UNC-5 act in the same pathway in a positive manner (i.e. *max-1* and *unc-5* have similar phenotypes that are enhanced in double mutant combinations). Our results analyzing growth cone morphology suggest that MAX-1 and UNC-5 might have opposing roles in growth cone protrusion, with MAX-1 normally attenuating UNC-5 signaling to allow for growth cone protrusion. How these interactions in the growth cone translate to endpoint axon guidance errors is unclear at this point. However, they do point to multiple and complex roles for these molecules in growth cones as they extend. While *max-1* suppresses excessive protrusion in *unc-5(hypomorphic)* mutants, the endpoint axon guidance phenotype is synergistically enhanced in the double mutant. This could be because we only analyzed VD growth cones and effects are different in DD growth cones. More likely is the possibility the roles of these molecules in the growth cone is complex, and that some effects of these mutants on growth cone morphology are being missed in this analysis. For example, speed of outgrowth and internal cytoskeletal and endosomal organization was not being assessed here. In any event, these results suggest that in growth cone protrusion, MAX-1 normally inhibits UNC-5 activity, allowing for robust growth cone protrusion necessary for proper VD axon guidance.

An UNC-6/Netrin-mediated balance of protrusive forces in the growth cone

Previous studies demonstrated that UNC-6/Netrin signaling mediates a balance of protrusive forces in the growth cone. UNC-5 homodimers and UNC-40/UNC-5 heterodimers inhibit growth cone protrusion in response to UNC-6, whereas UNC-40 homodimers stimulate protrusion in response to UNC-6 (Norris and Lundquist 2011; Norris et al. 2014; Gujar et al. 2018). UNC-5 and UNC-40/UNC-5 inhibit protrusion through the FMO flavin monooxygenases that might destabilize actin and through UNC-33/CRMP, which prevents microtubule + end entry into the growth cone thus preventing entry of pro-protrusive vesicles. The Rac GTPases CED-10 and MIG-2 are involved in both pathways. UNC-40 stimulates protrusion, possibly through the TIAM-1 GEF, the Rac GTPases CED-10 and MIG-2, and actin regulators such as the Arp2/3 complex and UNC-34/Enabled (Norris et al. 2009; Norris and Lundquist 2011; Demarco et al. 2012). This balance is demonstrated by the observation that the excess growth cone protrusion in *unc-5* mutants requires functional UNC-40 (i.e. in an *unc-5* mutant, UNC-40-driven protrusion is not counterbalanced by UNC-5 inhibition of protrusion, resulting in overly protrusive growth cones).

Work presented here suggests that the PH/MyTH4/FERM myosin-like protein MAX-1 participates in regulation of protrusion by inhibiting UNC-5. *max-1* growth cones are smaller and less protrusive than wild type, similar to constitutively activated *myr::unc-5*. Furthermore, *max-1* suppressed the excess growth cone protrusion in *unc-5* hypomorphic mutants, possibly by allowing residual UNC-5 function in these mutants to inhibit protrusion.

Data availability

All strains and reagents are available upon request. The data underlying this article are all available in the article.

Funding

This work was funded by R03NS114554 and R56NS095682 to EAL from the National Institutes of Neurological Disorders and Stroke; the National Institutes of Health Center for Molecular Analysis of Disease Pathways Genome Sequencing Core (P20GM103638); and the National Institutes of Health Kansas Infrastructure Network of Biomedical Research Excellence (P20GM103418).

Conflicts of interest

The authors report no conflicts of interest.

Literature cited

Brenner S. The genetics of *Caenorhabditis elegans*. Genetics. 1974; 77(1):71–94.

Chen S-Y, Ho C-T, Liu W-W, Lucanic M, Shih H-M, Huang P-H, Cheng H-J. Regulation of axon repulsion by MAX-1 SUMOylation and AP-3. Proc Natl Acad Sci USA. 2018;115(35):E8236–E8245.

Demarco RS, Struckhoff EC, Lundquist EA. The Rac GTP exchange factor TIAM-1 acts with CDC-42 and the guidance receptor UNC-40/DCC in neuronal protrusion and axon guidance. PLoS Genet. 2012;8(4):e1002665.

Gujar MR, Stricker AM, Lundquist EA. Flavin monooxygenases regulate *Caenorhabditis elegans* axon guidance and growth cone protrusion with UNC-6/Netrin signaling and Rac GTPases. PLoS Genet. 2017;13(8):e1006998.

Gujar MR, Stricker AM, Lundquist EA. RHO-1 and the Rho GEF RHGF-1 interact with UNC-6/Netrin signaling to regulate growth cone protrusion and microtubule organization in *Caenorhabditis elegans*. PLoS Genet. 2019;15(6):e1007960.

Gujar MR, Sundararajan L, Stricker A, Lundquist EA. Control of growth cone polarity, microtubule accumulation, and protrusion by UNC-6/Netrin and its receptors in *Caenorhabditis elegans*. Genetics. 2018;210(1):235–255.

Hedgecock EM, Culotti JG, Hall DH. The UNC-5, UNC-6, and UNC-40 genes guide circumferential migrations of pioneer axons and mesodermal cells on the epidermis in *C. elegans*. Neuron. 1990;4(1):61–85.

Huang X, Cheng HJ, Tessier-Lavigne M, Jin Y. MAX-1, a novel PH/MyTH4/FERM domain cytoplasmic protein implicated in netrin-mediated axon repulsion. Neuron. 2002;34(4):563–576.

Ishii N, Wadsworth WG, Stern BD, Culotti JG, Hedgecock EM. UNC-6, a laminin-related protein, guides cell and pioneer axon migrations in *C. elegans*. Neuron. 1992;9(5):873–881.

Jin Y, Jorgensen E, Hartwieg E, Horvitz HR. The *Caenorhabditis elegans* gene UNC-25 encodes glutamic acid decarboxylase and is required for synaptic transmission but not synaptic development. J Neurosci. 1999;19(2):539–548.

Killeen M, Tong J, Krizus A, Steven R, Scott I, Pawson T, Culotti J. UNC-5 function requires phosphorylation of cytoplasmic tyrosine 482, but its UNC-40-independent functions also require a region between the ZU-5 and death domains. Dev Biol. 2002;251(2):348–366.

Lim YS, Wadsworth WG. Identification of domains of netrin UNC-6 that mediate attractive and repulsive guidance and responses from cells and growth cones. J Neurosci. 2002;22(16):7080–7087.

Lowery LA, Van Vactor D. The trip of the tip: understanding the growth cone machinery. Nat Rev Mol Cell Biol. 2009;10(5):332–343.

Merz DC, Zheng H, Killeen MT, Krizus A, Culotti JG. Multiple signaling mechanisms of the UNC-6/Netrin receptors UNC-5 and UNC-40/DCC in vivo. Genetics. 2001;158(3):1071–1080.

Norris AD, Dyer JO, Lundquist EA. The Arp2/3 complex, UNC-115/abLIM, and UNC-34/Enabled regulate axon guidance and growth cone filopodia formation in *Caenorhabditis elegans*. Neural Dev. 2009;4:38.

Norris AD, Lundquist EA. UNC-6/netrin and its receptors UNC-5 and UNC-40/DCC modulate growth cone protrusion in vivo in *C. elegans*. Development. 2011;138(20):4433–4442.

Norris AD, Sundararajan L, Morgan DE, Roberts ZJ, Lundquist EA. The UNC-6/Netrin receptors UNC-40/DCC and UNC-5 inhibit growth cone filopodial protrusion via UNC-73/Trio, Rac-like GTPases and UNC-33/CRMP. Development. 2014;141(22):4395–4405.

Pak CW, Flynn KC, Bamburg JR. Actin-binding proteins take the reins in growth cones. Nat Rev Neurosci. 2008;9(2):136–147.

Tessier-Lavigne M, Goodman CS. The molecular biology of axon guidance. Science. 1996;274(5290):1123–1133.

Zhong H, Wu X, Huang H, Fan Q, Zhu Z, Lin S. Vertebrate MAX-1 is required for vascular patterning in zebrafish. Proc Natl Acad Sci USA. 2006;103(45):16800–16805.

Zhou FQ, Cohan CS. How actin filaments and microtubules steer growth cones to their targets. J Neurobiol. 2004;58(1):84–91.

Communicating editor: R. Pocock